Improving stress shielding following total hip arthroplasty by using a femoral stem made of β type Ti-33.6Nb-4Sn with a Young's modulus gradation

Go Yamako, Dennis Janssen, Shuji Hanada, Thomas Anijs, Kiyohide Ochiai, Koji Totoribe, Etsuo Chosa, Nico Verdonschot

PII: S0021-9290(17)30429-3
DOI: http://dx.doi.org/10.1016/j.jbiomech.2017.08.017
Reference: BM 8343

To appear in: *Journal of Biomechanics*

Accepted Date: 14 August 2017

Please cite this article as: G. Yamako, D. Janssen, S. Hanada, T. Anijs, K. Ochiai, K. Totoribe, E. Chosa, N. Verdonschot, Improving stress shielding following total hip arthroplasty by using a femoral stem made of β type Ti-33.6Nb-4Sn with a Young's modulus gradation, *Journal of Biomechanics* (2017), doi: http://dx.doi.org/10.1016/j.jbiomech.2017.08.017

Original Article

Improving stress shielding following total hip arthroplasty by using a femoral stem made of β type Ti-33.6Nb-4Sn with a Young's modulus gradation

Go Yamako [1]*, Dennis Janssen [2], Shuji Hanada [3], Thomas Anijs [2], Kiyohide Ochiai [4], Koji Totoribe, Etsuo Chosa [5], Nico Verdonschot [2,6]

1. Organization for Promotion of Tenure Track, University of Miyazaki, Miyazaki, Japan
2. Radboud University Medical Center, Radboud Institute for Health Sciences, Nijmegen, The Netherlands
3. Institute for Materials Research, Tohoku University, Sendai, Japan
4. Mizuho Corporation, Tokyo, Japan
5. Department of Medicine of Sensory and Motor Organs, Division of Orthopedic Surgery, Faculty of Medicine, University of Miyazaki, Miyazaki, Japan
6. University of Twente, Laboratory for Biomechanical Engineering, Faculty of Engineering Technology, Enschede, The Netherlands

*__Corresponding Author:__ Go Yamako, PhD
Organization for Promotion of Tenure Track, University of Miyazaki
1-1 Gakuen Kibana-dai-Nishi, Miyazaki, 889-2192, Japan
Tel/Fax: +81-985-58-7332
E-mail address: g.yamako@cc.miyazaki-u.ac.jp

Word count: 3996 words

Abstract

Stress shielding-related bone loss occurs after total hip arthroplasty because the stiffness of metallic implants differs from that of the host femur. Although reducing stem stiffness can ameliorate the bone resorption, it increases stress at the bone–implant interface and can inhibit fixation. To overcome this complication, a novel cementless stem with a gradient in Young's modulus was developed using Ti-33.6Nb-4Sn (TNS) alloy. Local heat treatment applied at the neck region for increasing its strength resulted in a gradual decrease in Young's modulus from the proximal to the distal end, from 82.1 to 51.0 GPa as calculated by a heat transfer simulation. The Young's modulus gradient did not induce the excessive interface stress which may cause the surface debonding. The main purpose of this study was to evaluate bone remodeling with the TNS stem using a strain-adaptive bone remodeling simulation based on finite element analysis. Our predictions showed that, for the TNS stem, bone reduction in the calcar region (Gruen zone 7) would be 13.6% at 2 years, 29.0% at 5 years, and 45.8% at 10 years postoperatively. At 10 years, the bone mineral density for the TNS stem would be 42.6% higher than that for the similar Ti-6Al-4V alloy stem. The stress–strength ratio would be lower for the TNS stem than for

the Ti-6Al-4V stem. These results suggest that although proximal bone loss cannot be eliminated completely, the TNS stem with a Young's modulus gradient may have bone-preserving effects and sufficient stem strength, without the excessive interface stress.

Key words: Total hip arthroplasty, Stress shielding, Low modulus stem, Bone remodeling, Finite element analysis

1. Introduction

Total hip arthroplasty (THA) is one of the most beneficial procedures in orthopedic surgery (Learmonth et al., 2007), but subsequent femoral bone remodeling can affect long-term clinical performance. Severe proximal bone resorption can reduce implant stability, causing subsidence and aseptic loosening, which can result in periprosthetic fracture and complex revision surgery (Engh et al., 2003; Lindahl, 2007; Taylor and Tanner, 1997; Wilkinson et al., 2003). The etiology of proximal bone loss is multifactorial (Sychterz and Engh, 1996), but the main cause is a reduction in the load transmitted to the bone, so-called "stress shielding" (Huiskes, 1990; Van Rietbergen et al., 1993), with the femur remodeling to accommodate the new mechanical situation (Bobyn et al., 1992; Engh et al., 1999). Various types of femoral stems have been tried, including anatomic, straight, wedge-taper, customized, and short-type stems; nevertheless, stress shielding continues to occur in most cases (Bieger et al., 2012; Khanuja et al., 2011).

The main reason for stress shielding is the difference in stiffness between the implant and the host bone (Head et al., 1995; Huiskes et al., 1992), which causes stresses to

be transferred predominantly through the implant. Low-modulus isoelastic stems were first introduced 40 years ago to reduce stress shielding (Bombelli and Mathys, 1982; Katoozian et al., 2001; Morscher et al., 1981; Skinner, 1991), but inadequate bone fixation and fatigue failure of the plastic materials led to a high failure rate (Adam et al., 2002; Jakim et al., 1988; Morscher and Dick, 1983; Niinimaki et al., 1994; Runne et al., 1989; Trebse et al., 2005). Although reducing stem stiffness can prevent severe bone resorption, biomechanical studies have shown that this change increases bone–implant interface stresses, which may cause interface debonding and may inhibit biological fixation, resulting in loosening (Huiskes et al., 1992; Kuiper and Huiskes, 1996; Weinans et al., 1992). Thus, two incompatible design goals exist with regard to femoral stems.

To solve these two conflicting demands, Kuiper and Huiskes (1997) proposed a femoral stem with a non-homogeneous distributed Young's modulus using numerical design optimization methods. In a simplified optimized model of a hip stem, the interface stress was reduced by >50% compared with that of a stem with a homogeneously low modulus.

Following this concept, Hanada et al. (2014) were the first to develop a novel cementless stem with a gradation of Young's modulus, using the newly designed β-type Ti-33.6Nb-4Sn alloy (the "TNS stem," Fig. 1a). Local heat treatment, applied at the femoral neck region, increased stem strength, compared to a conventional Ti-6Al-4V alloy, and gradually decreased Young's modulus, from proximal to distal regions due to low thermal conductivity. Young's modulus and alloy strength depend on the heat treat temperature through fine α precipitation in the fiber structure. Our *in vitro* biomechanical study of the TNS stem demonstrated a proximal load-transfer pattern and good initial stability (Yamako et al., 2014). However, it is unclear if the TNS stem can reduce stress shielding-induced bone loss.

To predict bone adaptive responses after THA, Huiskes et al. (1987) developed a coupling finite element (FE) model with algorithms of bone remodeling, based on a mechanical stimulus. This model uses strain energy density (SED) as a stimulus to determine the rate of bone formation and resorption, and is widely used to study implant designs (Sumner, 2015). In this study, we compared femoral bone remodeling and the stress

state of reconstructions with the TNS stem and with a similar Ti-6Al-4V alloy stem, using the adaptive bone remodeling simulation based on FE analysis.

2. Materials and methods

The distributions of Young's modulus and strength in the TNS stem were based on a thermal FE simulation of the heat-treatment temperature, combined with known relations between the temperature and the material properties. The femoral neck region was locally heated to 693 K for 5 hours in a N_2 gas atmosphere to increase the strength of the neck region. The heat treatment induced a temperature gradation that was monitored using 10 thermocouples inserted into 0.7 mm-diameter holes drilled in the stem surface.

The final temperature distribution was simulated using thermal FE analyses to determine the Young's modulus and tensile strength distributions (Marc 2007, MSC Software Corporation, CA, USA). The stem model consisted of 42,866 four-node tetrahedral elements, and was also used for the bone remodeling simulation described later. The thermal properties of the Ti-33.6Nb-4Sn alloy are listed in Table 1. The atmosphere

temperature and initial temperature of the TNS stem were set to 300 K and the surface of the neck region was heated locally at 693 K for 5 hours. The remaining stem surface was defined as a heat transfer area. The transient thermal analysis was validated against the measured values. For the subsequent bone remodeling simulation, we established the temperature-dependent Young's modulus and tensile strength distributions for the TNS stem, based on fourth-order polynomial curve fits to the temperature–material property relationships (Fig. 1b), derived from previous tensile tests (Hanada et al., 2014).

To validate the mechanical response of the TNS stem model with an estimated Young's modulus distribution, we compared the axial stiffness of the TNS stem determined from the structural FE analysis with that from the experiment. The stiffness was examined under an axial compressive loading using a material testing machine. The distal region of the stem was clamped to two steel tapered V-shaped flute blocks. The working length of the stem, from the top of the block to the center of the femoral head, was set at 140 mm. A load was applied to the femoral head, up to a maximum of 1200 N (crosshead speed = 1.0 mm/min). The loading direction was parallel to the long axis of the stem. The slope of

load-displacement curve was used to estimate the stiffness of the TNS stem. We performed a structural FE simulation of the TNS stem to estimate the axial stiffness. The Poisson' ratio was set to 0.3. The distal clamping region was fully fixed. An axial load was applied to a node, at the center position of the head. The center node was rigid-linked to the tapered neck region of the TNS stem. We performed linear elastic analysis to calculate the displacement of the center node, and then determined the axial stiffness.

To evaluate the newly developed TNS stem, we performed a validated FE method-based bone remodeling simulation (Tarala et al., 2011). The FE model of the femur was created from CT data of an 81-year-old man's left femur, scanned with a calibration phantom (Image Analysis, Columbia, KY, USA), and processed using Mimics® (Materialise, Leuven, Belgium). We then generated FE models of femurs implanted with the TNS and Ti-6Al-4V stems, positioned in the virtual bones by an experienced surgeon. The geometry of the Ti-6Al-4V stem was the same as the TNS stem. The proximal two-thirds of each femur with the stem was meshed with four-noded tetrahedral elements with a mean edge

length of 2 mm, with a node-to-node bone–stem interface (Mentat 2015, MSC Software Corporation, CA, USA). The model consisted of 74,540 and 42,866 elements for the bone and the stem, respectively (Fig. 2a). The bone and stems assigned with isotropic, linearly elastic properties. The bone stiffness was derived from calibrated CT data. The Hounsfield Units were converted to calcium-equivalent densities (ρ_{CHA}) for each element, after which the ash density was computed ($\rho_{ash} = 0.0633 + 0.887\rho_{CHA}$). The Young's modulus was then computed based on the ash density (ρ_{ash}) using correlations for trabecular and cortical bone (Keyak and Falkinstein, 2003). In the present study, we used an ash-to-apparent density ratio (ρ_{ash}/ρ_{app}) of 0.6 over the whole density range (Schileo et al., 2008). The Ti-6Al-4V stem had a Young's modulus of 110 GPa and a tensile strength to 860 MPa. The Young's modulus and tensile strength of the TNS stem were based on the thermal analysis described above (Fig. 2b). Poisson's ratio for the bone and implants was set to 0.3. The grit-blasted area at the stem–bone interface was assumed to be bonded. The remaining smooth area was defined as having frictional contact ($\mu = 0.3$) (ten Broeke et al., 2014).

We applied the strain-adaptive bone remodeling theory to simulate changes in

bone mineral density with time ($d\rho/dt$) (Huiskes et al., 1987; Weinans et al., 1992). The stimulus (S) for bone remodeling was the difference between the preoperative (R_{ref}) and postoperative local SED, unless S was within a "dead zone" ([$(1 - D) \times R_{ref}$, $(1 + D) \times R_{ref}$], where D is the dead zone value) in which no remodeling occurred ($d\rho/dt = 0$). When S was smaller or greater than the dead zone, bone resorption or apposition, respectively, took place. The remodeling signal was averaged over the three loading conditions ($S = (S_1 + S_2 + S_3)/3$), in which the femur was subjected to normal walking and stair climbing (Fig. 2a, Table 2). Normal walking consisted of two peak hip joint forces (beginning and end of the single stance phase), stair climbing was represented by the peak force during a stair climbing cycle (Heller et al., 2001). The rate of mass change depended on the density as a measure for available free bone surface (Martin, 1984). Time in the remodeling simulation (computer time unit, ctu) depended on the maximum stimulus per iteration: the greater the stimulus, the smaller the time iteration. The size of the dead zone (0.35) and the ctu (60, corresponding to two real-world years) were determined in our previous study, which utilized the same bone model (Tarala et al., 2011).

For a clinically relevant interpretation, we projected the bone remodeling results onto 2D virtual dual energy X-ray absorptiometry (DEXA) images. We defined seven Gruen zones (Gruen et al., 1979), and computed the bone mineral density (BMD, g/cm^2) for each stem for up to ten years postoperatively. The change in BMD predicted by our simulations was expressed as a percentage of the preoperative BMD.

We also compared changes in the stress states of the TNS and Ti-6Al-4V stems and femurs under stair climbing loading. To evaluate the structural strength of the stems, their Von Mises stress–tensile strength ratios (SSRs) were calculated.

3. Results

The predicted temperature ranged from 523 K at the distal tip to 693 K in the proximal region (Fig. 3). The relative errors between the predicted and measured temperatures at ten measuring points are listed in Table 3. The mean relative error was 1.5% and the root mean square error was 11 K. The range in Young's modulus for the TNS stem, calculated from the temperature distribution, was 51.0–82.1 GPa (Fig. 2b). The

tensile strength ranged from 997.5 MPa at the distal tip to 1290.7 MPa at the neck region.

In the axial compression test, the load-displacement curve showed a linear response (R^2=0.99, Fig3c). The axial stiffness of the TNS stem, determined from the FE analysis and the experiment, were 577.2 and 585.4 N/mm, respectively (relative error = 1.4%).

The remodeling simulation showed that the TNS stem resulted in lower bone resorption than the Ti-6Al-4V stem in almost all Gruen zones (Fig. 4). The BMD in each Gruen zone was represented as a percentage of the BMD immediately after the operation (i.e., before remodeling). The greatest decreases in BMD were predicted to occur during the first 5 years, with small changes continuing for both stems. Bone loss occurred mainly in the proximal part of the femur (Gruen zones 1, 6, and 7). The greatest bone resorption was observed in Gruen zone 7 (up to 62.0% for the Ti-6Al-4V stem and 45.8% for the TNS stem at 10 years). In Gruen zone 6, the BMD of the TNS stem was almost preserved up to 10 years (96.4%). The difference in BMD between the stems increased gradually with time

in the proximal regions. In particular, in Gruen zone 7, the difference in BMD was 4.6% at 2 years (Ti-6Al-4V stem: 81.8%; TNS stem: 86.4%), 10.8% at 5 years (Ti-6Al-4V stem: 60.2%; TNS stem: 71.0%), and 16.2% at 10 years (Ti-6Al-4V stem: 38.0%; TNS stem: 54.2%). In contrast, only small differences were observed at 10 years in Gruen zones 1 (5.6%) and 2 (3.0%).

For both stems, dense areas appeared at the border between the grit-blasted and the smooth surface and stem tip; clinically, this is referred to as a "spot weld" and "pedestal formation" (Fig. 5).

As a measure for the interface stresses at the grid-blasted region, we took Von Mises stresses at the surface nodes of the bone. The peak interface stress appeared at the proximal edge on the medial side (Ti-6Al-4V stem: 24.3 MPa; TNS stem: 30.3 MPa), immediately after the operation. The mean (SD) values of the interface stress for the Ti-6Al-4V and TNS were 2.6 (3.0) and 3.0 (3.6) MPa, respectively. The mean interface stress for the Ti-6Al-4V and TNS stems increased to 118% and 125%, respectively, at 5

years postoperatively, and to 121% and 130% at 10 years.

The von Mises stress in the reconstruction with the TNS stem was greater than that with the Ti-6Al-4V stem, especially in the calcar region (Fig. 6a). Bone remodeling after the operation changed the stress states of the femur and stem over time. In both stems, the bone adaptation led to a decrease in stress in the proximal region and an increase in the distal region. In the calcar region (representative nodes are indicated by arrows in Fig. 6a), the von Mises stress for the TNS stem decreased linearly from 9.1 MPa immediately after surgery to 1.3 MPa at 10 years (Fig. 6b). The stress for the TNS stem was greater than that for the Ti-6Al-4V stem throughout this period.

Similar distributions of SSR were observed in both stems even though SSR depends on the stress state, Young's modulus, and the tensile strength (Fig.7a). The maximum SSR occurred in the neck region in both stems (Ti-6Al-4V stem: 0.26; TNS stem: 0.17). Bone remodeling increased the SSR slightly with time in the middle and distal regions of the stem. In the middle region, the SSRs for the Ti-6Al-4V and TNS stems increased to 127% and 124%, respectively, at 5 years postoperatively, and to 148% and

141% at 10 years (Fig. 7b). SSRs for the Ti-6Al-4V stem were greater than the TNS stem throughout the 10 years.

4. Discussion

The TNS stem was designed to promote proximal loading and thus to reduce proximal bone loss through the gradation of Young's modulus. The present study showed that Young's modulus in TNS stem ranged continuously from 82.1 GPa proximally to 51.0 GPa at the distal tip, as calculated using our heat transfer simulation with sufficient accuracy. The FE simulation showed that the bone stress in the calcar region in the immediate postoperative period was 18% higher with the TNS stem than with the Ti-6Al-4V stem, indicating greater proximal loading in the TNS stem. Similar load-transfer patterns for a femur implanted with the TNS stem were observed in a previous *in vitro* experimental study (Yamako et al., 2014). The interface stress for the TNS stem was comparable to that of the Ti-6Al-4V stem. Therefore, the Young's modulus gradient prevents excessive increases in the interface stress, as described by Kuiper and Huiskes

(1997). Since the bonding strength of the Ti-Nb-Sn alloy was equal to that of the Ti-6Al-4V alloy (Miura et al., 2011), we could expect secure fixation for the TNS stem.

The main purpose of the present study was to evaluate bone remodeling of the TNS stem using strain-adaptive bone remodeling theory. Our predictions showed that bone loss occurred mainly in the proximal parts of both implanted femurs, with the greatest bone resorption in the calcar region (Gruen zone 7). These bone remodeling patterns were consistent with previous bone remodeling studies with different stems (Dickinson, 2014; Herrera et al., 2007; Tarala et al., 2011; Tavakkoli Avval et al., 2015; ten Broeke et al., 2014). In addition, the pedestal formation and spot welds similar to those seen clinically appeared in the simulation models. In Gruen zone 7, the BMD for the TNS stem was 42.6% higher than that for the Ti-6Al-4V stem at 10 years, indicating that the TNS stem could reduce femoral bone loss compared to the conventional Ti-6Al-4V stem. However, because the TNS stem did not reproduce the physiological stress state in the femur, bone resorption could not be completely eliminated.

Our simulations suggest that the TNS stem may exhibit certain bone-preserving

effects. In particular, the BMD in Gruen zone 7 decreased by 13.6% at 2 years and 45.8% at 10 years. A previous study using the same bone and remodeling parameters predicted that the BMD in the Epoch® stem would decrease by 27.5% at 2 years and 75.0% at 10 years (Tarala et al., 2011). The Epoch® stem is a successful, low-stiffness stem for which long-term clinical performance has been reported (Hartzband et al., 2010; Thien et al., 2012): proximal bone loss with this stem has been shown to be less than that associated with a more rigid stem design (Glassman et al., 2001; Karrholm et al., 2002). However, the bone-sparing effect remains controversial. Dual X-ray absorptiometry has demonstrated that the greatest decrease in mean bone density (27.5%) occurred in the calcar region at 2 years (Akhavan et al., 2006). A possible reason for this bone loss is that the Epoch® stem is fully porous-coated around the stem, which affects the security of fixation against increased interface stress. However, this is likely to promote distal load transfer and to result in proximal stress shielding. The degree of stress shielding is affected by the bonding conditions of the implant–bone interface (Huiskes, 1990).

With both stems, adaptive bone remodeling after implantation changed the stress

state in the femur and stem. Over time, the bone stress decreased gradually in the calcar region but increased in the distal region. In both stems, the stresses at the middle and distal portions increased simultaneously. These changes indicate that the stem support moved distally due to the proximal bone loss, i.e., the bone remodeling increased the severity of bending for both stems. We therefore calculated SSR to evaluate the strength of the stems under stair climbing loads, because of the non-homogeneous distribution of the tensile strength in the TNS stem. Our results showed that the SSRs in the middle region of the Ti-6Al-4V and TNS stems increased to 148% and 141%, respectively, at 10 years. Across all regions of the stem, the SSRs of the TNS stem were lower than those of the Ti-6Al-4V stem. Thus, the TNS stem may be at lower risk for failure than the Ti-6Al-4V stem. The TNS stem has already passed the fatigue performance test (ISO 7206-4 and 7206-6), which require that it is able to resist dynamic cyclic loading without fracture to verify its endurance properties. The TNS stem is currently in use in clinical trial.

The TNS stem allows control of the structural stiffness and strength through heat treatment. The TNS stem has a conical tapered shape. This stem type is widely used in

clinical practice, with excellent long-term results (Khanuja et al., 2011), but may cause proximal stress shielding in 50%–88% of cases (Bourne et al., 2001; Park et al., 2003). Additionally, mild-to-moderate activity-related thigh pain in 4% of the patients has been reported (Bourne et al., 2001). Thigh pain may also occur after THA, and its origin may be related to the relatively high stem bending stiffness (Brown et al., 2002; Hartzband et al., 2010). This stem type seems to be an appropriate choice for reducing Young's modulus and thus reducing both stress shielding and thigh pain. The heat treatment conditions increased neck region strength and accomplished the Young's modulus gradient. Hanada et al. (2014) demonstrated the distribution of Young's modulus in the TNS stem using the Vickers hardness test. Yamako et al. (2014) confirmed a gradual decrease in the Young's modulus of the TNS stem, from the proximal to the distal region, using cantilever bending tests. In present study, we established a simulation model of the TNS stem, including the temperature-dependent Young's modulus and validated the axial stiffness.

In our simulation, the majority of bone loss occurred during the first 5 years, with small changes afterward. At 10 years the predicted bone loss in the calcar region appeared

high. We do not know if adaptive bone remodeling continues, or stops after a certain time. Most changes of the BMD, around cementless stems, occur in the first 2 years (Bugbee et al., 1997). However, recent clinical studies report long-term remodeling (Boden et al., 2006; Li et al., 2007; McCarthy et al., 1991; Merle et al., 2011). Mueller et al. (2010) reported decreases in cortical and cancellous bone density, especially in the calcar region between the one and six year examinations. Panisello et al. (2009) reported progressive bone loss in Gruen zone seven up to 42.9% at 10 years for an anatomic stem. The bone loss continued to progress at seven years and the bone-sparing effect persisted in only the calcar region for the Epoch® stem (Thien et al., 2012). Long-term bone remodeling can be predicted by FE based simulations (Dickinson, 2014; Herrera et al., 2007; Tarala et al., 2011). However, further clinical studies on the DEXA are needed to evaluate the long-term bone remodeling for the TNS stem.

Our bone remodeling simulation included assumptions that should be noted as limitations. First, we recognize that bone remodeling in the femur after THA has a multifactorial origin (Sychterz and Engh, 1996). Adaptive bone remodeling only uses strain

energy density as the stimulus to drive bone remodeling, while others have suggested other stimuli should be included, such as microdamage (Scannell and Prendergast, 2009), stress non-uniformity (Adachi et al., 2001), biochemical reactions (Tavakkoli Avval et al., 2015) and biological processes (Huiskes et al., 2000). Second, the loading condition in our simulation was constant in the preoperative and postoperative condition. In reality, patients become active after surgery. Dickinson (2014) demonstrated the importance of load and activity factors when predicting bone remodeling. Third, the remodeling rule was limited to the internal remodeling without correction for geometrical changes. Fourth, we assumed a perfect bond between the stem and bone, at the grit-blasted surface. Although for cementless stems the initial fixation is provided by friction and pre-stress at the roughed interface generated by a press-fit implantation, our models did not include the press-fit condition. This ideal interface condition could underestimate the effect of stress shielding.

However, since bone remodeling is long term process, other studies did not take into account bone ingrowth processes and press-fit conditions after surgery (Huiskes et al., 1992; Lerch et al., 2012; Tavakkoli Avval et al., 2015). For instance, a porous Tantalum

surface achieves an almost complete bone ingrowth within 16 weeks with little changes after one year (Bobyn et al., 1999). Incorporating these issues as mathematical models after the validation of the simulations would improve the accuracy of the bone remodeling in the model and then, could make patient-specific predictions of bone loss. It should also be noted that we simulated remodeling around only one bone model implanted with stems. Although the selected femur was considered to be average in terms of shape, size, and BMD, the results could be influenced by bone quality and the implant position in the intramedullary canal. However, because the same bone model was used for two stems, our FE simulations allowed us to make comparisons regarding the effects of material properties on bone remodeling.

In conclusion, this strain-adaptive bone remodeling simulation showed that, although proximal femoral bone loss mediated by stress shielding was not eliminated completely, the new TNS stem with a gradation of Young's modulus exhibited bone-preserving effects and sufficient stem strength, without the excessive interface stress. The flexibility and strength of the novel, low-modulus Ti-33.6Nb-4Sn alloy can easily be

controlled using heat treatment, and it may represent a candidate biomaterial for manufacturing cementless femoral stems to replace those made from the conventional Ti-6Al-4V alloy. In future studies, we will focus on the optimization of the heat treatment conditions and the shape of the stem with the aim of minimizing stress shielding.

Conflict of interest statement

All authors state that there are no conflicts of interest, which might influence the preparation of this manuscript. One of the authors is under employment of Mizuho Corporation, Tokyo, Japan. The Mizuho played no role in the interpretation of results.

Acknowledgements

This work was supported by JSPS KAKENHI Grant Numbers JP15KK0213 and a grant from the Program to Disseminate Tenure Tracking System from the Ministry of Education, Culture, Sports, Science, and Technology of Japan.

References

Adachi, T., Tsubota, K., Tomita, Y., Hollister, S.J., 2001. Trabecular surface remodeling simulation for cancellous bone using microstructural voxel finite element models. Journal of Biomechanical Engineering 123, 403-409.

Adam, F., Hammer, D.S., Pfautsch, S., Westermann, K., 2002. Early failure of a press-fit carbon fiber hip prosthesis with a smooth surface. The Journal of Arthroplasty 17, 217-223.

Akhavan, S., Matthiesen, M.M., Schulte, L., Penoyar, T., Kraay, M.J., Rimnac, C.M., Goldberg, V.M., 2006. Clinical and histologic results related to a low-modulus composite total hip replacement stem. The Journal of Bone and Joint Surgery, American Volume 88, 1308-1314.

Bieger, R., Ignatius, A., Decking, R., Claes, L., Reichel, H., Durselen, L., 2012. Primary stability and strain distribution of cementless hip stems as a function of implant design. Clinical Biomechanics 27, 158-164.

Bobyn, J.D., Mortimer, E.S., Glassman, A.H., Engh, C.A., Miller, J.E., Brooks, C.E., 1992.

Producing and avoiding stress shielding. Laboratory and clinical observations of noncemented total hip arthroplasty. Clinical Orthopaedics and Related Research 274, 79-96.

Bobyn, J.D., Stackpool, G.J., Hacking, S.A., Tanzer, M., Krygier, J.J., 1999. Characteristics of bone ingrowth and interface mechanics of a new porous tantalum biomaterial. The Journal of Bone and Joint Surgery, British Volume 81, 907-914.

Boden, H.S., Skoldenberg, O.G., Salemyr, M.O., Lundberg, H.J., Adolphson, P.Y., 2006. Continuous bone loss around a tapered uncemented femoral stem: a long-term evaluation with DEXA. Acta Orthopaedica 77, 877-885.

Bombelli, R., Mathys, R., 1982. Cementless isoelastic RM total hip prosthesis. Journal of the Royal Society of Medicine 75, 588-597.

Bourne, R.B., Rorabeck, C.H., Patterson, J.J., Guerin, J., 2001. Tapered titanium cementless total hip replacements: a 10- to 13-year followup study. Clinical Orthopaedics and Related Research 393, 112-120.

Brown, T.E., Larson, B., Shen, F., Moskal, J.T., 2002. Thigh pain after cementless total hip

arthroplasty: evaluation and management. The Journal of the American Academy of Orthopaedic Surgeons 10, 385-392.

Bugbee, W.D., Culpepper, W.J., 2nd, Engh, C.A., Jr., Engh, C.A., Sr., 1997. Long-term clinical consequences of stress-shielding after total hip arthroplasty without cement. The Journal of Bone and Joint Surgery, American Volume 79, 1007-1012.

Dickinson, A.S., 2014. Activity and loading influence the predicted bone remodeling around cemented hip replacements. Journal of Biomechanical Engineering 136.

Engh, C.A., Jr., Sychterz, C., Engh, C., Sr., 1999. Factors affecting femoral bone remodeling after cementless total hip arthroplasty. The Journal of Arthroplasty 14, 637-644.

Engh, C.A., Jr., Young, A.M., Engh, C.A., Sr., Hopper, R.H., Jr., 2003. Clinical consequences of stress shielding after porous-coated total hip arthroplasty. Clinical Orthopaedics and Related Research 417, 157-163.

Glassman, A.H., Crowninshield, R.D., Schenck, R., Herberts, P., 2001. A low stiffness composite biologically fixed prosthesis. Clinical Orthopaedics and Related Research 393, 128-136.

Gruen, T.A., McNeice, G.M., Amstutz, H.C., 1979. "Modes of failure" of cemented stem-type femoral components: a radiographic analysis of loosening. Clinical Orthopaedics and Related Research 141, 17-27.

Hanada, S., Masahashi, N., Jung, T.K., Yamada, N., Yamako, G., Itoi, E., 2014. Fabrication of a high-performance hip prosthetic stem using beta Ti-33.6Nb-4Sn. Journal of the Mechanical Behavior of Biomedical Materials 30, 140-149.

Hartzband, M.A., Glassman, A.H., Goldberg, V.M., Jordan, L.R., Crowninshield, R.D., Fricka, K.B., Jordan, L.C., 2010. Survivorship of a low-stiffness extensively porous-coated femoral stem at 10 years. Clinical Orthopaedics and Related Research 468, 433-440.

Head, W.C., Bauk, D.J., Emerson, R.H., Jr., 1995. Titanium as the material of choice for cementless femoral components in total hip arthroplasty. Clinical Orthopaedics and Related Research 311, 85-90.

Heller, M.O., Bergmann, G., Deuretzbacher, G., Durselen, L., Pohl, M., Claes, L., Haas, N.P., Duda, G.N., 2001. Musculo-skeletal loading conditions at the hip during walking and stair climbing. Journal of Biomechanics 34, 883-893.

Herrera, A., Panisello, J.J., Ibarz, E., Cegonino, J., Puertolas, J.A., Gracia, L., 2007. Long-term study of bone remodelling after femoral stem: a comparison between dexa and finite element simulation. Journal of Biomechanics 40, 3615-3625.

Huiskes, R., 1990. The various stress patterns of press-fit, ingrown, and cemented femoral stems. Clinical Orthopaedics and Related Research 261, 27-38.

Huiskes, R., Ruimerman, R., van Lenthe, G.H., Janssen, J.D., 2000. Effects of mechanical forces on maintenance and adaptation of form in trabecular bone. Nature 405, 704-706.

Huiskes, R., Weinans, H., Grootenboer, H.J., Dalstra, M., Fudala, B., Slooff, T.J., 1987. Adaptive bone-remodeling theory applied to prosthetic-design analysis. Journal of Biomechanics 20, 1135-1150.

Huiskes, R., Weinans, H., van Rietbergen, B., 1992. The relationship between stress shielding and bone resorption around total hip stems and the effects of flexible materials. Clinical Orthopaedics and Related Research 274, 124-134.

Jakim, I., Barlin, C., Sweet, M.B., 1988. RM isoelastic total hip arthroplasty. A review of 34 cases. The Journal of Arthroplasty 3, 191-199.

Karrholm, J., Anderberg, C., Snorrason, F., Thanner, J., Langeland, N., Malchau, H., Herberts, P., 2002. Evaluation of a femoral stem with reduced stiffness. A randomized study with use of radiostereometry and bone densitometry. The Journal of Bone and Joint Surgery, American Volume 84, 1651-1658.

Katoozian, H., Davy, D.T., Arshi, A., Saadati, U., 2001. Material optimization of femoral component of total hip prosthesis using fiber reinforced polymeric composites. Medical Engineering & Physics 23, 503-509.

Keyak, J.H., Falkinstein, Y., 2003. Comparison of in situ and in vitro CT scan-based finite element model predictions of proximal femoral fracture load. Medical Engineering & Physics 25, 781-787.

Khanuja, H.S., Vakil, J.J., Goddard, M.S., Mont, M.A., 2011. Cementless femoral fixation in total hip arthroplasty. The Journal of Bone and Joint Surgery, American Volume 93, 500-509.

Kuiper, J.H., Huiskes, R., 1996. Friction and stem stiffness affect dynamic interface motion in total hip replacement. Journal of Orthopaedic Research 14, 36-43.

Kuiper, J.H., Huiskes, R., 1997. Mathematical optimization of elastic properties: application to cementless hip stem design. Journal of Biomechanical Engineering 119, 166-174.

Learmonth, I.D., Young, C., Rorabeck, C., 2007. The operation of the century: total hip replacement. Lancet 370, 1508-1519.

Lerch, M., Kurtz, A., Stukenborg-Colsman, C., Nolte, I., Weigel, N., Bouguecha, A., Behrens, B.A., 2012. Bone remodeling after total hip arthroplasty with a short stemmed metaphyseal loading implant: finite element analysis validated by a prospective DEXA investigation. Journal of Orthopaedic Research 30, 1822-1829.

Li, M.G., Rohrl, S.M., Wood, D.J., Nivbrant, B., 2007. Periprosthetic changes in bone mineral density in 5 stem designs 5 years after cemented total hip arthroplasty. No relation to stem migration. The Journal of Arthroplasty 22, 689-691.

Lindahl, H., 2007. Epidemiology of periprosthetic femur fracture around a total hip arthroplasty. Injury 38, 651-654.

Martin, R.B., 1984. Porosity and Specific Surface of Bone. Critical Reviews in Biomedical

Engineering 10, 179-222.

McCarthy, C.K., Steinberg, G.G., Agren, M., Leahey, D., Wyman, E., Baran, D.T., 1991. Quantifying bone loss from the proximal femur after total hip arthroplasty. The Journal of Bone and Joint Surgery, British Volume 73, 774-778.

Merle, C., Streit, M.R., Volz, C., Pritsch, M., Gotterbarm, T., Aldinger, P.R., 2011. Bone remodeling around stable uncemented titanium stems during the second decade after total hip arthroplasty: a DXA study at 12 and 17 years. Osteoporosis International 22, 2879-2886.

Miura, K., Yamada, N., Hanada, S., Jung, T.K., Itoi, E., 2011. The bone tissue compatibility of a new Ti-Nb-Sn alloy with a low Young's modulus. Acta Biomaterialia 7, 2320-2326.

Morscher, E., Bombelli, R., Schenk, R., Mathys, R., 1981. The treatment of femoral neck fractures with an isoelastic endoprosthesis implanted without bone cement. Archives of Orthopaedic and Trauma Surgery 98, 93-100.

Morscher, E.W., Dick, W., 1983. Cementless fixation of "isoelastic" hip endoprostheses manufactured from plastic materials. Clinical Orthopaedics and Related Research 176,

77-87.

Mueller, L.A., Nowak, T.E., Haeberle, L., Mueller, L.P., Kress, A., Voelk, M., Pfander, D., Forst, R., Schmidt, R., 2010. Progressive femoral cortical and cancellous bone density loss after uncemented tapered-design stem fixation. Acta Orthopaedica 81, 171-177.

Niinimaki, T., Puranen, J., Jalovaara, P., 1994. Total hip arthroplasty using isoelastic femoral stems. A seven- to nine-year follow-up in 108 patients. The Journal of Bone and Joint Surgery, British Volume 76, 413-418.

Panisello, J.J., Herrero, L., Canales, V., Herrera, A., Martinez, A.A., Mateo, J., 2009. Long-term remodeling in proximal femur around a hydroxyapatite-coated anatomic stem: ten years densitometric follow-up. The Journal of Arthroplasty 24, 56-64.

Park, M.S., Choi, B.W., Kim, S.J., Park, J.H., 2003. Plasma spray-coated Ti femoral component for cementless total hip arthroplasty. The Journal of Arthroplasty 18, 626-630.

Runne, W.C., van Sambeek, K.J., Stierum, J.L., van Tongerloo, R.B., 1989. Femoral endoprosthesis fixation with a soft, flexible low modulus stem coating. Four to six year clinical results. Orthopedics 12, 529-535.

Scannell, P.T., Prendergast, P.J., 2009. Cortical and interfacial bone changes around a non-cemented hip implant: simulations using a combined strain/damage remodelling algorithm. Medical Engineering & Physics 31, 477-488.

Skinner, H.B., 1991. Isoelasticity and total hip arthroplasty. Orthopedics 14, 323-328.

Sumner, D.R., 2015. Long-term implant fixation and stress-shielding in total hip replacement. Journal of Biomechanics 48, 797-800.

Sychterz, C.J., Engh, C.A., 1996. The influence of clinical factors on periprosthetic bone remodeling. Clinical Orthopaedics and Related Research 322, 285-292.

Tarala, M., Janssen, D., Verdonschot, N., 2011. Balancing incompatible endoprosthetic design goals: a combined ingrowth and bone remodeling simulation. Medical Engineering & Physics 33, 374-380.

Tavakkoli Avval, P., Samiezadeh, S., Klika, V., Bougherara, H., 2015. Investigating stress shielding spanned by biomimetic polymer-composite vs. metallic hip stem: A computational study using mechano-biochemical model. Journal of the Mechanical Behavior of Biomedical Materials 41, 56-67.

Taylor, M., Tanner, K.E., 1997. Fatigue failure of cancellous bone: a possible cause of implant migration and loosening. The Journal of Bone and Joint Surgery, British Volume 79, 181-182.

ten Broeke, R.H., Tarala, M., Arts, J.J., Janssen, D.W., Verdonschot, N., Geesink, R.G., 2014. Improving peri-prosthetic bone adaptation around cementless hip stems: a clinical and finite element study. Medical Engineering & Physics 36, 345-353.

Thien, T.M., Thanner, J., Karrholm, J., 2012. Fixation and bone remodeling around a low-modulus stem seven-year follow-up of a randomized study with use of radiostereometry and dual-energy x-ray absorptiometer. The Journal of Arthroplasty 27, 134-142 e131.

Trebse, R., Milosev, I., Kovac, S., Mikek, M., Pisot, V., 2005. Poor results from the isoelastic total hip replacement: 14-17-year follow-up of 149 cementless prostheses. Acta Orthopaedica 76, 169-176.

Van Rietbergen, B., Huiskes, R., Weinans, H., Sumner, D.R., Turner, T.M., Galante, J.O., 1993. The mechanism of bone remodeling and resorption around press-fitted THA stems.

Journal of Biomechanics 26, 369-382.

Weinans, H., Huiskes, R., Grootenboer, H.J., 1992. The behavior of adaptive bone-remodeling simulation models. Journal of Biomechanics 25, 1425-1441.

Wilkinson, J.M., Hamer, A.J., Rogers, A., Stockley, I., Eastell, R., 2003. Bone mineral density and biochemical markers of bone turnover in aseptic loosening after total hip arthroplasty. Journal of Orthopaedic Research 21, 691-696.

Yamako, G., Chosa, E., Totoribe, K., Hanada, S., Masahashi, N., Yamada, N., Itoi, E., 2014. In-vitro biomechanical evaluation of stress shielding and initial stability of a low-modulus hip stem made of beta type Ti-33.6Nb-4Sn alloy. Medical Engineering & Physics 36, 1665-1671.

Tables

Table 1 Material properties of the Ti-33.6Nb-4Sn (TNS) stem for heat transfer analysis.

Mass density	5520	kg/m^3
Specific heat coefficient	451	J/(kg K)
Thermal conductivity	8.4	W/(m K)
Heat transfer coefficient	2.5	$W/(m^2 K)$

Table 2 Details of joint contacts and muscle force vector directions and magnitudes (N).

Load case		Walking (toe off)			Walking (heel strike)			Stair climbing		
Direction		F_x	F_y	F_z	F_x	F_y	F_z	F_x	F_y	F_z
P0	Hip contact	−432	−263	−1833	−342	29	−1575	−475	−485	−1890
P1	Abductors	518	122	646	375	6	369	664	237	618
P2	Vastus lateralis	−7	148	−743	0	0	0	−18	179	−1081
P3	Vastus medialis	0	0	0	0	0	0	−70	317	−2137

Table 3 Comparison of heat-treatment temperatures (K).

	Measuring point									
	1	2	3	4	5	6	7	8	9	10
Experiment	684	665	659	651	638	616	596	568	549	535
Finite element method	693	687	666	654	641	627	598	559	533	524
Relative error, %	1.3	3.3	1.1	0.5	0.5	1.9	0.4	1.6	2.9	2.0

Figure legends

Fig. 1 (a) The newly developed flexible cementless stem made from Ti-33.6Nb-4Sn alloy. The stem has conical tapered shape, with a proximal grit-blasted surface. (b) How Young's modulus and the tensile strength of the Ti-33.6Nb-4Sn alloy vary with heat treatment temperature.

Fig. 2 (a) Finite element model of the stem-implanted left femur. (b) Distribution of Young's modulus and the tensile strength in the TNS stem.

Fig. 3 (a) The temperature measuring points in the TNS stem. (b) The calculated temperature distribution. (c) Load-displacement curve: finite element method vs experimental tests.

Fig. 4 Changes in bone mineral density (BMD) in Gruen zones 1-7 relative to the immediate postoperative BMD (set at 100% as the baseline reference).

Fig. 5 Cross section showing the bone mineral density (BMD) distribution around the TNS stem immediately after the operation (post-op). BMD dense regions, the so-called "spot weld" (a) and "pedestal formation" (b), were observed 5 years postoperatively.

Fig. 6 (a) The von Mises stress distributions in the TNS and Ti-6Al-4V stems under stair climbing loading immediately after the operation (post-op) and at 5 years postoperatively. (b) Bone stresses at the points indicated by the arrows in (a) (node ID: 5834) decreased with time.

Fig. 7 (a) The distributions of stress–strength ratio (SSR) for the two stem types under stair climbing loading immediate after the operation (post-op) and 5 years postoperatively. (b) SSR changes with time at the neck, middle, and distal region of the stem (as indicated by the arrows in (a)).

(a)

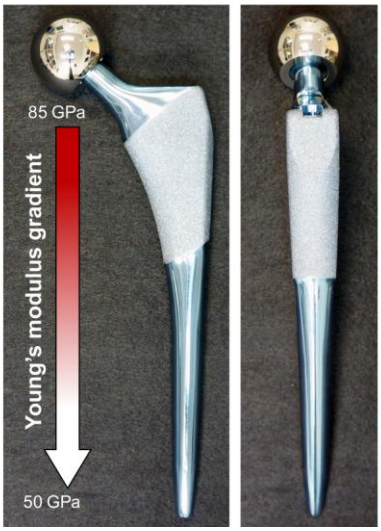

(b)